FUZZY OBJECT MODELING

Jayaram K. Udupa[a], Dewey Odhner[a], Alexandre X. Falcao[b], Krzysztof Chris Ciesielski[a,c], Paulo A.V. Miranda[b], Pavithra Vaideeswaran[a], Shipra, Mishra[a], George J. Grevera[a,d], Babak Saboury[e], Drew A. Torigian[e]
[a]Medical Image Processing Group (jay@mail.med.upenn.edu) - UPENN – Philadelphia, PA
[b]Institute of Computing – University of Campinas – Campinas, SP, Brazil
[c]Department of Mathematics – West Virginia University – Morgantown, WV
[d]Department of Mathematics and Computer Science – Saint Joseph's University – Philadelphia, PA
[e]Department of Radiology – Hospital of the University of Pennsylvania – Philadelphia, PA

ABSTRACT

To make Quantitative Radiology (*QR*) a reality in routine clinical practice, computerized automatic anatomy recognition (*AAR*) becomes essential. As part of this larger goal, we present in this paper a novel fuzzy strategy for building body-wide group-wise anatomic models. They have the potential to handle uncertainties and variability in anatomy naturally and to be integrated with the fuzzy connectedness framework for image segmentation. Our approach is to build a family of models, called the Virtual Quantitative Human, representing normal adult subjects at a chosen resolution of the population variables (gender, age). Models are represented hierarchically, the descendents representing organs contained in parent organs. Based on an index of fuzziness of the models, 32 thorax data sets, and 10 organs defined in them, we found that the hierarchical approach to modeling can effectively handle the non-linear relationships in position, scale, and orientation that exist among organs in different patients.

Keywords: anatomic models, segmentation, fuzzy objects, fuzzy connectedness

1. INTRODUCTION

Since the birth of radiology in 1895, the emphasis in clinical radiology has been on *human visualization* of internal structures. Since radiography could not unravel internal information in an unobscured manner, the continued quest for internal body visualization heralded various tomographic image modalities for deriving anatomic, functional, and molecular information. However, this emphasis on human visualization continued and the practice of *clinical radiology* has remained mostly *descriptive* and *subjective*. Quantification is amply employed in radiology in clinical research. However, in clinical radiological practice, this is rare. In this qualitative mode, quantifiable and/or subtle image information is underutilized, interpretations remain subjective, and subtle changes due to early disease or therapeutic intervention may be underestimated or missed [1]. If *QR* can be brought to routine clinical practice, numerous advances can be made ranging from: improved sensitivity, specificity, accuracy, and precision of early disease diagnosis; more objective and *standardized* response assessment of diseases to treatment; improved understanding of what is "normal"; increased ease of disease measurement and reporting; discovery of new disease biomarkers; effective handling of the large volume of image information; and effective combined utilization of multimodality image information.

We envision a *QR* system to operate in the following manner. Imagine we build a family of body-wide models, at a desired resolution of the population variables (gender, age), complete with anatomic, organ geographic, dynamic, physiological, and functional information. Supported by the model family, the implemented *QR* system will then automatically recognize and delineate the anatomy in the given patient image(s) during clinical image interpretation, highlight deviations from normality, and list a host of pertinent quantitative measures, indicating their normal range for the particular group to which the patient belongs, highlighting out-of-range measures if any.

To make *QR* a reality in routine clinical radiological practice, computerized *Automatic Anatomy Recognition* (*AAR*) during radiological image reading, therefore, becomes essential. To facilitate *AAR*, and hence *QR*, and focusing only on

Medical Imaging 2011: Visualization, Image-Guided Procedures, and Modeling,
edited by Kenneth H. Wong, David R. Holmes III, Proc. of SPIE Vol. 7964, 79640B

the anatomic aspects of shape, geography, and architecture of organs, but keeping the larger goal in mind, we present in this paper a novel fuzzy strategy for building anatomic models.

We think of image segmentation as consisting of two related phenomena: *Recognition* – the high-level process of determining the whereabouts of objects in the image, and *Delineation* – the low-level process of ascertaining the precise spatial occupation of objects in the image. Segmentation methods may be broadly classified into three groups: purely image-based (*pI*) approaches [2-9], shape model-based (*SM*) approaches [10-13], and the emerging hybrid approaches [14-17]. The *pI* approaches are powerful in delineation but need help in recognition. The *SM* approaches are strong in recognition but not as powerful in delineation. The hybrid approaches attempt to combine the delineation strengths of *pI* methods synergistically with the recognition capabilities of *SM* approaches. *SM* approaches become essential for *AAR*.

Our *QR* focus will be on the torso, especially the thorax. Considerable progress has already been made in the spirit of *AAR* in the brain [14, 15, 18, 19]. The challenges faced in building practical *AAR* systems for the brain and the rest of the body are quite unique to each of these areas. Recently, there has been a considerable increase in interest in *SM* approaches for body regions other than the brain. For example, in the *SPIE* 2009 and 2010 *Medical Imaging Conference Proceedings*, there were some 45 papers on this topic; all devoted to specific organs, image modalities, and disease conditions. A full scale *AAR* methodology to serve in *QR* for the body torso and extremities has not yet been developed. Therefore, the proposed methodology has significance in advancing *AAR* and *QR* for various non-neurological applications in the body.

Probabilistic and fuzzy techniques have been co-developed in different endeavors including image analysis and segmentation. Probabilistic/statistical techniques have been studied extensively for shape modeling under *SM* approaches, but little exists on fuzzy object modeling except our own earlier preliminary work [20, 21]. Therefore bringing fuzzy set concepts to object modeling is an innovative, fundamental contribution of this work. Fuzzy and probability principles start off with different axioms and use different mathematical constructs [22] and lead to very different algorithms in imaging. Our motivation for developing fuzzy object modeling principles is to find natural and computationally efficient means of bringing prior object shape information for large object assemblies into graph based *pI* approaches such as *FC*, live wire, watershed, and graph cut. Thus, our approach is inherently digital and fuzzy, without making continuous approximations or important assumptions on prior distributions and random phenomena, etc.

There are several components to the *AAR-QR* project we are pursuing: (C1) gathering body-wide group-wise image data for *normal* subjects; (C2) building fuzzy models and evaluating them; (C3) using fuzzy models to recognize and delineate anatomy in a given patient image set; (C4) detecting and delineating pathology; (C5) quantification; (C6) computational set up for interactive-rate performance. In this paper, our focus is only on (C2) – constructing fuzzy models and their evaluation – which forms one of the core aspects of the whole effort.

2. FUZZY MODELS

Let B denote a *body region* of interest, and $\mathcal{C} = \langle C, f \rangle$ denote an *image* acquired for B, where $C \subset Z^3$ is the *domain* of $\mathcal{C}$ covering B, and f: $C \rightarrow$ R is the image *intensity* function. The elements of C will be called voxels and the values of $f(v)$ for any $v \in C$ will be referred to as the intensity of voxel v. Let $\mathcal{C}_1,\ldots,\mathcal{C}_N$ be the images of B for N subjects, all belonging to a particular group G (defined by a chosen resolution of the population variables), which are provided for building the model for B. *The fuzzy organ model* for B, denoted $FOM(B)$, is a quadruple $FOM(B) = \langle H, \mathcal{M}, \rho, \lambda \rangle$. Briefly, H denotes a hierarchy, expressed as a tree, of the organs and the sub-organs in B. $\mathcal{M}$ is a family of fuzzy sets $\mathcal{M} = \{FM_\ell : 1 \leq \ell \leq L\}$, each member representing one of L organs/sub-organs of B as a fuzzy set over the subject population. ρ denotes parent-to-offspring relationship in the hierarchy over H and N subjects. λ is a family $\{\lambda_\ell : 1 \leq \ell \leq L\}$ of L scale factor ranges $\lambda_\ell = [\lambda_\ell^a, \lambda_\ell^b]$, indicating the size variation of the organs in B over N subjects. Once $FOM(B)$ is built, it can be used to perform *AAR* in any image $\mathcal{C}$ acquired for B of any new subject (patient) who belongs to the same group as G. We will require that the set of images $\{\mathcal{C}_1,\ldots,\mathcal{C}_N\}$ provided for model building all pertain to subjects whose body region B is normal.

The model building process consists of the following three steps:

Step 1. Gathering image data:

The cleanest way of gathering image data for model building is to prospectively acquire image data from subjects certified to be normal under each group *G* at an adequate "resolution" of the group variables (gender, age, etc.). Such an approach would be an expensive and labor intensive undertaking. For developing the concepts and testing the feasibility, we have taken a vastly less expensive and simpler approach of utilizing existing patient data. The two radiologists participating in this project (*BS*, *DAT*) examined all image data and certified them to be radiologically normal for the body region for which they are considered. In this manner, we have collected 32 contrast enhanced *CT* (breath-hold) image data sets from 32 patients from our hospital database for the thorax and similarly 52 data sets for the abdomen. For now, we have considered only male subjects in the age range of 50-60 for these data. Our modeling schema is such that the population variables can be defined at higher "resolutions" in the future, and the model updated when more data are added.

Step 2. Delineating organ boundaries:

In this paper, we will focus mainly on the thoracic body region and major organs in the thorax, with the hierarchy (*H*) as illustrated in Fig. 1. Let *L* denote the number of organs (in this case, $L = 11$).

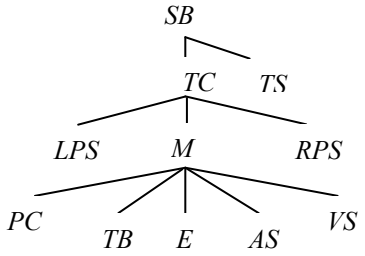

Figure 1: Hierarchy of thoracic organs. *SB*: Skin Boundary; *TC:* Thoracic Cavity; *TS:* Thoracic Skeleton*; LPS*: Left Plural Sac; *M*: Mediastinum; *RPS*: Right Plural Sac; *PC*: Pericardium; *TB*: Trachea & Bronchi; *E*: Esophagus; *AS*: Arterial System; *VS*: Venous System.

In body-wide modeling, a tree such as the one in Fig. 1 becomes a sub-tree of a tree associated with the whole body, each sub-tree corresponding to a different body region.

Each of the *L* organs is delineated in each of the images in the set $\{\mathcal{C}_n = \langle C_n, f_n \rangle : 1 \le n \le N\}$ to generate a family of binary images $S = \{\mathcal{C}_{n,\ell} = \langle C_{n,\ell}, f_n, \ell \rangle : 1 \le n \le N,\ 1 \le \ell \le L\}$. Each $\mathcal{C}_{n,\ell}$ represents the region occupied by the organ in its image domain rather than indicating just the boundary. The delineation is done by employing a combination of tools and under the guidance and verification of the two radiologists.

Step 3: Constructing fuzzy models:

Let $O_1,....,O_L$ be the organs considered in B to be included in the fuzzy model. In our case $O_1 = SB,\ O_2 = TC,\ O_3 = TS$, *etc*., see Fig. 1. Let $S_\ell = \{\mathcal{C}_{n,\ell} :\ 1 \le n \le N\}$ be the set of binary images representing object O_ℓ in the *N* different subjects in group *G*. Ideally, for any $1 \le \ell \le L$, we would like the different samples of O_ℓ in different subjects to differ by a homothetic affine transformation (translation, rotation, and isotropic scaling) $A_{n,\ell}$. Our idea behind the concept of a fuzzy model is to codify the spatial variations in shape from this ideal that may exist among the *N* samples as a spatial fuzzy set, while also retaining the spatial relationship among objects in the hierarchical order.

The fuzzy object model of O_ℓ will be denoted by FM_ℓ, and expressed as a fuzzy subset of a reference set $\Omega_\ell \subset Z^3$, defined in the Scanner Coordinate System (*SCS*); that is, $FM_\ell = (\Omega_\ell, \mu_\ell)$. The membership function $\mu_\ell(v),\ v \in \Omega_\ell$ defines the degree of membership of voxel *v* in the model of O_ℓ. Further details on how $A_{n,\ell}$, μ_ℓ, and FM_ℓ are determined from the set S_ℓ of binary images are given below.

We permit only such alignment operations, mimicking $A_{n,\ell}$, among the members of S_ℓ, that are executed precisely and that avoid the uncertainties of local optima associated with optimization-based full-fledged registration schemas. In this spirit, we handle the translation, rotation, and scaling components of $A_{n,\ell}$ in the following manner.

For translation and rotation, for each manifestation of O_ℓ in $\mathcal{C}_{n,\ell}, 1 \le n \le N$, we determine, within *SCS*, the geometric center and the inertia (principal) axes of O_ℓ from the region occupied by O_ℓ in $\mathcal{C}_{n,\ell}$. Subsequently, all samples are aligned to the mean center and axes. These translation and rotation operations may also be determined based on some reference object such as *TS*, in which case, these operations will be identical for all objects within the same subject.

The scale factor estimation is based on a linear size estimate (in *mms*) of each sample of O_ℓ and resizing all samples to the mean size. Five methods of size estimation are tested: (m_1) $\left(V_{n,\ell}\right)^{1/3}$ where $V_{n,\ell}$ is the volume of O_ℓ in $\mathcal{C}_{n,\ell}$. (m_2) The diagonal length of the smallest box enclosing O_ℓ in $\mathcal{C}_{n,\ell}$ whose edges are parallel to the image coordinate axes. (m_3) $\left(\lambda_{n,\ell}\right)^{1/2}$ where $\lambda_{n,\ell}$ is the eigenvalue associated with the major principal axis of O_ℓ in $\mathcal{C}_{n,\ell}$. (m_4) The diagonal length of the box enclosing the skeleton (*TS*) in $\mathcal{C}_{n,\ell}$. ($m5$) The diagonal length of the box enclosing the union of all objects excluding *SB* in $\mathcal{C}_{n,\ell}$ (this object will be denoted by ALL for future reference). Note that $m1$-$m3$ constitute object-dependent scaling. That is, in these strategies, for any fixed ℓ, the samples of O_ℓ are scaled based on the mean size of O_ℓ estimated from its family. In $m4$ and $m5$, all objects in a given subject are scaled uniformly by using the scale factors derived from the family of objects *TS* and ALL, respectively. For this scale factor estimation, any of the measures under $m1$-$m3$ may be employed to determine the size of *TS* and ALL. For example, in $m4$ based on *TS*, and employing the measure of size in $m1$, the mean of $\left(V_{n,\ell}\right)^{1/3}$ over all samples of O_ℓ = *TS* is determined first. This mean size is then utilized to scale not just *TS* in each subject *n* but also his all other objects.

There are several possible scenarios of combining the methods used for scaling, translation, and rotation. In this paper, we will study three scenarios, denoted $S1$-$S3$, for understanding the quality of the resulting fuzzy models. In $S1$, all operations are object specific. That is, for any object O_ℓ, its sample in each $\mathcal{C}_{n,\ell}$ is translated, rotated, and scaled based on the mean center, orientation, and size (determined by one of the methods $m1$-$m3$) estimated from all samples of O_ℓ only. In $S2$, the means are estimated based on *TS*. Then all objects O_ℓ, $1 \le \ell, \le L$ for a given subject *n* undergo the same translation, rotation, and scaling as determined by the *TS* for that subject. $S3$ is similar to $S2$ except that, in place of *TS*, we use ALL.

Since we deal with digital images, an interpolant is needed to derive $A_{n,\ell}\left(\mathcal{C}_{n,\ell}\right)$. Since $\mathcal{C}_{n,\ell}$ are binary images, we employ the shape-based interpolating scheme [23], which first applies a distance transform *DT* [24] to the boundary of the object in $\mathcal{C}_{n,\ell}$, resulting in a (gray level) image *DT* ($\mathcal{C}_{n,\ell}$) to which an appropriate (such as tri-linear) interpolating function $I_{n,\ell}$ is applied to derive another gray-level image denoted $\mathcal{C}^a_{n,\ell} = \left\langle C^a_{n,\ell}, f^a_{n,\ell} \right\rangle$.

The aligned binary images, denoted $\mathcal{C}^{a,b}_{n,\ell} = \left\langle C^a_{n,\ell}, f^{a,b}_{n,\ell} \right\rangle$, corresponding to O_ℓ, are obtained by thresholding $\mathcal{C}^a_{n,\ell}$ at 0 (meaning $f^{a,b}_{n,\ell}(v) = 1$ if $f^a_{n,\ell}(v) \ge 0$; otherwise $f^{a,b}_{n,\ell}(v) = 0, v \in C^a_{n,\ell}$). *DT* assigns to voxels inside O_ℓ in $\mathcal{C}_{n,\ell}$ a positive distance value, and to those outside, a negative value. Since *DT* propagates shape information inside and outside the boundary of O_ℓ in $\mathcal{C}_{n,\ell}$, it is useful in both (shape-based) interpolation and in deriving FM_ℓ. The fuzzy model $FM_\ell = \left(\Omega_\ell, \mu_\ell\right)$ is such that, for any $v \in \Omega_\ell$,

$$\mu_\ell(v) = g\left(\left[f^a_{n,\ell}(v)\right] / N\right).$$

Ω_ℓ is taken to be the smallest set (rectangular array) of voxels such that

$$\Omega_\ell \supset \bigcup_{n=1}^{N} C_{n,\ell}^{a},$$

and g is a sigmoid function that maps distance values into fuzzy membership values in [0, 1]. In words, the aligned and shape-interpolated distance maps of the different manifestations of O_ℓ in the family are averaged. Then averaged distance values are mapped to [0, 1].

Our *AAR* approach makes essential use of the hierarchy information and parent-to-offspring relationship encapsulated in ρ. For each valid pair (ℓ, k) such that O_ℓ and O_k are a parent object and an offspring, $\rho_{\ell,k}$ codifies the mean positional relationship $P_{\ell,k}$ between O_ℓ and O_k and its variation $V_{\ell,k}$ over N samples. We adopt the convention that $\rho_{0,1}$ stores information about the mean positional relationship of the root object *SB* relative to *SCS*. Let $GC_{n,\ell}$ be the geometric center of O_ℓ in $\mathcal{C}_{n,\ell}$, $1 \le n \le N$, $1 \le \ell \le L$. Then $P_{\ell,k}$ is the mean of the vectors in the set $\{GC_{n,k} - GC_{n,\ell} : 1 \le n \le N\}$ and $V_{\ell,k}$ is a 2nd order tensor, obtained via *PCA* of this set. In order not to corrupt $\rho_{\ell,k}$ by the differences in size among subjects, before estimating $\rho_{\ell,k}$, O_ℓ and all offspring objects O_k of O_ℓ are scaled with respect to the center $GC_{n,\ell}$ of O_ℓ as per a common scale factor, estimated for O_ℓ via one of methods *m*1-*m*3. The reason behind this process is the thinking that an object and all its offsprings should be scaled similarly to retain their positional relationship information correctly.

There are several choices for the operations and their parameters in building the fuzzy models. We would like these to be selected in such a manner that, without changing the shape of the sample objects or affecting the relationship among objects, the model created is as crisp as possible. We characterize the crispness of a fuzzy model by an entity called the *index of fuzziness*. We employ the following measure of index of fuzziness of a fuzzy model FM_ℓ, which is derived directly from the aligned binary images $\mathcal{C}_{n,\ell}^{a,b}$:

$$h(FM_\ell) = 1 - \frac{\left| \bigcap_n \mathcal{C}_{n,\ell}^{a,b} \right|}{\left| \bigcup_n \mathcal{C}_{n,\ell}^{a,b} \right|}.$$

Here $\bigcap$ and $\bigcup$ denote logical intersection and union operations on binary images. $\mathcal{M}$, H, ρ, and λ serve a variety of purposes in *AAR*. For example, in recognizing and delineating objects in a given image $\mathcal{C}$, a synergistic integration of the fuzzy models, the variability in $V_{\ell,k}$, and the fuzzy connectedness machinery [25] is carried out to first locate in $\mathcal{C}$ an object that is easy to recognize, such as *SB*. The hierarchical organization then imposes severe constraints on the subsequent recognition and delineation tasks guided by the object segmented so far, which also provides a scale estimate (from λ) and a positional estimate (from ρ) for the objects to be segmented subsequently. The model concepts also generalize readily to spaces higher than three-dimensional. Thus, static as well as dynamic objects and their mixtures can be modeled within the same framework. These topics will be the subject matter of our future work. In the next section, we will analyze empirically the model building process for the thoracic body region in some detail.

3. EXPERIMENTAL ANALYSIS

The results presented in this section are for the thorax image data. As mentioned earlier, these images are collected from our patient image database of routine clinical scans which are of clinical spatial resolution (typical voxel size of $0.9 \times 0.9 \times 5\ mm^3$). We will demonstrate a justification for the hierarchical concept in *FOM*(*B*), not from the perspective of *AAR* (although this is obviously very important, but, for now, outside the scope of this paper), but from the consideration of the quality of the resulting models.

Fig. 2 displays the cross-sectional boundaries of the 3D surfaces of all N samples for three of the 11 objects - *LPS*, *M*, and *PC* - upon alignment. In Fig. 2(a), the N members of the object family are aligned by the object specific method *S*1

with scaling via m_1 for creating $FOM(B)$. In 2(b) and 2(c), similarly, the corresponding object cross sections for methods $S2$ and $S3$ are displayed. From these displays and many other similar cross sections we have examined, we note that object-specific translation, rotation, and scaling achieves better alignment. We may conclude that object-specific alignment is important to produce crisper *FOMs*. In Fig. (3a), we show surface renditions of some of the objects in B for one subject. In 3(b), volume renditions of $FOM(B)$ with some object models suppressed for minimizing obscuration, are shown, all based on the $m1$ measure. It is important to note that the renditions also depict the correct (mean) ρ and λ parameters, in the true spirit of the meaning of $FOM(B)$.

(a)

(b)

(c)

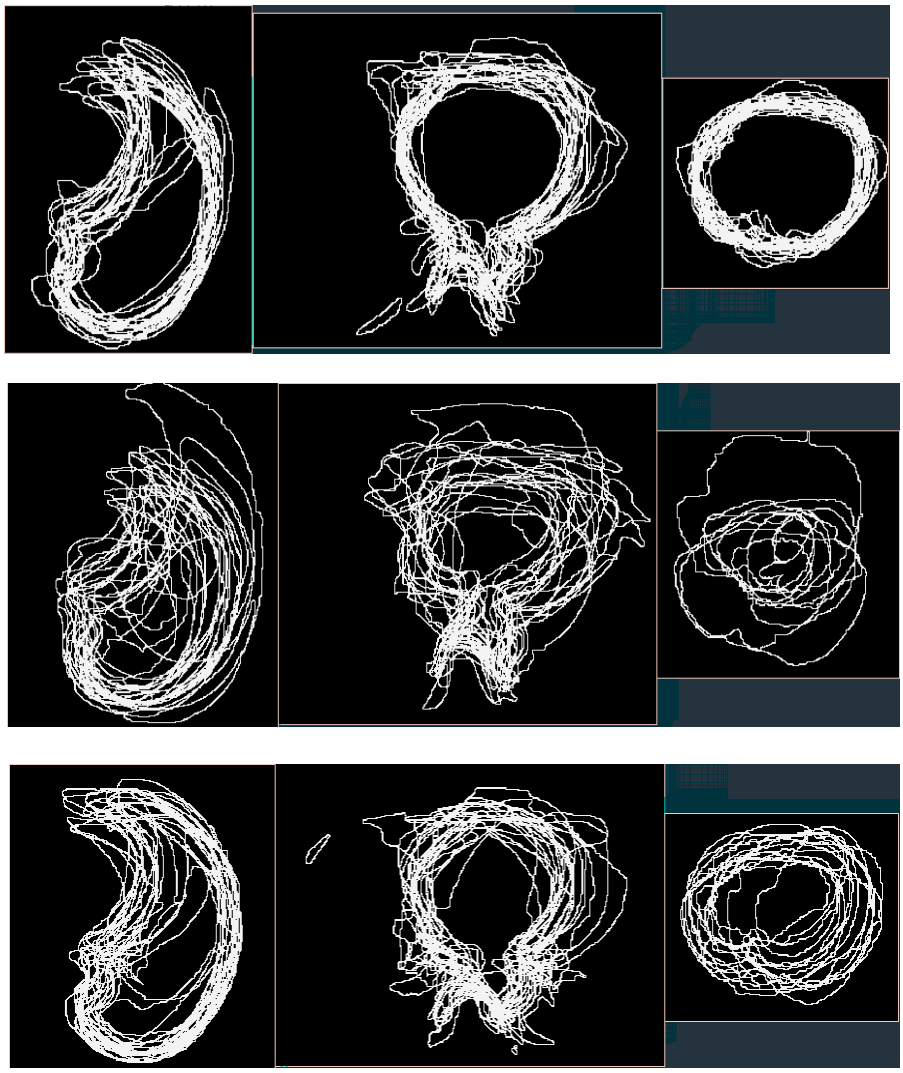

Figure 2: Cross sections of the aligned objects *LPS*, *PC*, and *TB* based on the $m1$ measure for scenario $S1$ (a), $S2$ (b), and $S3$ (c).

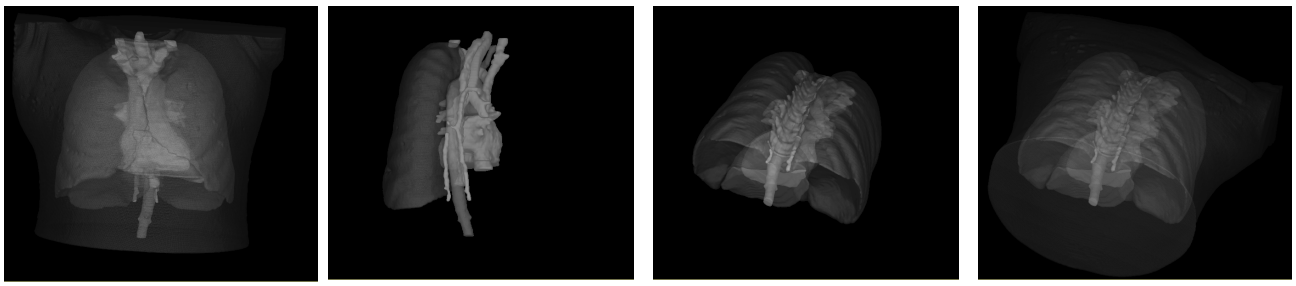

(a)

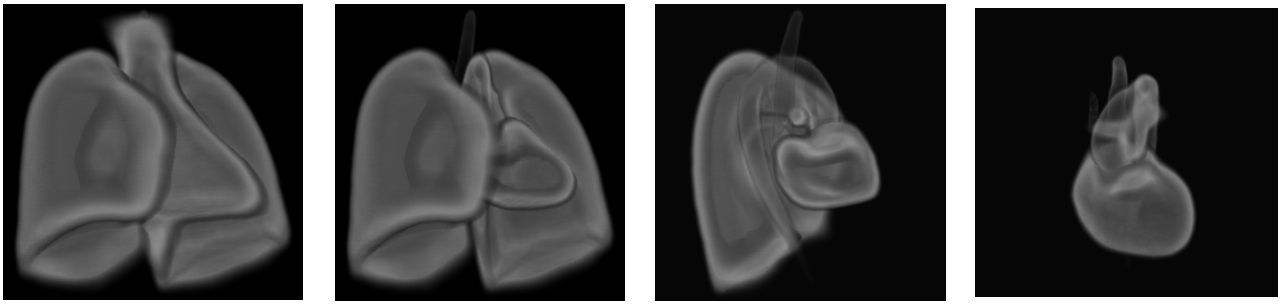

(b)

Figure 3: (a) Surface renditions of some of the 11 objects from one of the *N* subjects. (b) Volume renditions of *FOM*(*B*) derived via *m*1 for scenario *S*1. Different combinations of object models FM_ℓ are shown.

Table 1 lists some summary statistics for the linear measures m_1-m_3 used for scale estimation for the different objects. Note that the statistics listed under *TS* and ALL correspond respectively to measures *m*4 and *m*5. Note also that there is no definite pattern in the values of *CV* for *m*1-*m*3 for the different objects. Generally *m*3 shows larger variations among members of the same object family than *m*2 and *m*1.

		AS	*E*	*LPS*	*M*	*PC*	*RPS*	*SB*	*TB*	*VS*	*TS*	ALL
	MEAN	67.15	35.54	130.37	120.69	84.67	137.20	295.21	36.67	45.21	83.41	193.27
***m* 1**	***SD***	4.61	4.01	14.36	6.55	6.55	13.20	13.99	3.45	5.20	6.14	13.19
	CV	6.86	11.28	11.01	5.43	7.74	9.62	4.74	9.41	11.49	7.37	6.82
	MEAN	353.47	237.15	351.97	383.93	198.82	359.08	603.73	191.15	300.34	525.28	526.05
***m* 2**	***SD***	31.73	24.67	27.69	33.26	13.86	31.73	35.03	18.24	21.80	31.29	31.90
	CV	8.98	10.40	7.87	8.66	6.97	8.84	5.80	9.54	7.26	5.96	6.06
	MEAN	67.60	68.78	59.29	60.55	32.05	56.28	103.76	45.12	60.75	96.49	70.13
***m* 3**	***SD***	8.46	8.39	7.03	6.58	2.82	7.40	6.71	3.71	7.90	8.73	4.17
	CV	12.52	12.20	11.85	10.86	8.81	13.14	6.47	8.23	13.00	9.05	5.94

Table 1: Summary statistics of the sizes of objects derived via *m*1, *m*2, and *m*3 over the subject population. All units are in *mms*, except C*V* (coefficient of variation), which is expressed as percent.

Tables 2 and 3 display the residual size variation left over in each object family after uniform scaling of all members of each object family by measures m_4 and m_5 specific to each family, respectively. Note that, in object-dependent scaling by measures *m*1-*m*3, residual size variation is 0. Table 4 lists the correlation coefficients of the object dependent scale factors between different objects based on the m_1 measure. A high correlation would indicate that object-dependent scaling can be replaced by uniform scaling. This is counter indicated in the table except for some obvious pairs like *LPS* and *RPS*. The data in Tables 2, 3, and 4 provide a strong justification for object-dependent scaling and alignment. We emphasize that it is not just a matter of registering the members of each object family optimally by employing a 7-parameter (3 translations + 3 rotations + 1 scaling) transformation. For the hierarchical recognition and delineation of all objects in the *AAR* approach, it is important to account for the hierarchical relationship information ρ and the concomitant scale information λ properly as outlined in Step 3 in the previous section. If we attempt to solve this problem via a single image registration operation, it will lead to a registration problem with 7*LN* free parameters; that is, the search space becomes 7*LN*-dimensional (which amounts to 2464 even in the relatively small *AAR* problem we have undertaken). The approach we proposed is an approximate solution to this very complex problem.

		AS	*E*	*LPS*	*M*	*PC*	*RPS*	*SB*	*TB*	*VS*	*ALL*
	MEAN	67.36	35.62	131.10	121.22	84.96	137.94	296.91	36.79	45.31	194.19
***m* 1**	***SD***	5.11	3.86	17.81	9.91	7.39	17.04	27.99	3.70	4.73	18.71
	CV	7.59	10.82	13.58	8.17	8.69	12.35	9.43	10.07	10.43	9.63
	MEAN	353.31	237.45	352.95	385.01	199.20	360.12	604.59	191.12	300.87	526.40
***m* 2**	***SD***	21.47	23.29	30.98	36.82	14.74	35.26	32.16	13.43	22.01	2.79
	CV	6.08	9.81	8.78	9.56	7.40	9.79	5.32	7.03	7.32	0.53
	MEAN	67.51	69.02	59.47	60.79	32.36	56.45	104.19	45.29	61.13	70.63
***m* 3**	***SD***	4.55	8.01	6.33	6.33	4.58	6.62	7.27	3.55	8.87	7.08
	CV	6.74	11.60	10.64	10.41	14.17	11.73	6.98	7.84	14.50	10.03

Table 2: Residual object size variation left over (*SD* & *CV*) after alignment based on *TS* with object-independent scaling via *m*1, *m*2, amd *m*3. All units are in *mms*, except C*V* (coefficient of variation), which is expressed as percent.

		AS	*E*	*LPS*	*M*	*PC*	*RPS*	*SB*	*TB*	*VS*	**TS**
	MEAN	67.44	35.67	130.01	121.11	85.06	136.95	296.34	36.66	45.37	83.74
***m* 1**	***SD***	6.36	4.30	6.94	9.00	8.94	5.23	22.35	2.20	5.65	8.18
	CV	9.43	12.06	5.34	7.43	10.51	3.82	7.54	6.00	12.45	9.77
	MEAN	353.32	237.43	352.96	385.01	199.22	360.13	604.65	191.10	300.89	526.02
***m* 2**	***SD***	21.18	22.98	30.89	36.43	14.84	35.14	32.62	12.94	22.11	2.79
	CV	5.99	9.68	8.75	9.46	7.45	9.76	5.40	6.77	7.35	0.53
	MEAN	67.81	68.65	59.16	60.52	32.12	56.17	103.93	45.19	60.73	96.75
***m* 3**	***SD***	9.39	5.83	4.63	5.09	3.10	5.76	6.87	3.54	6.87	9.93
	CV	13.85	8.49	7.82	8.41	9.65	10.26	6.61	7.83	11.31	10.26

Table 3: Residual object size variation left over (*SD* & *CV*) after object-independent alignment based on ALL with scaling via *m*1, *m*2, and *m*3. All units are in *mms*, except C*V* (coefficient of variation), which is expressed as percent.

	AS	*E*	*LPS*	*M*	*PC*	*RPS*	*SB*	*TB*	*VS*	*TS*	**ALL**
AS	1.00	0.23	-0.03	0.68	0.65	-0.03	0.05	0.15	0.32	0.50	0.13
E	0.23	1.00	0.11	0.39	0.32	0.10	0.13	0.20	0.22	0.36	0.20
LPS	-0.03	0.11	1.00	0.16	-0.13	0.98	0.26	0.73	0.06	0.03	0.97
M	0.68	0.39	0.16	1.00	0.74	0.16	0.48	0.34	0.29	0.32	0.36
PC	0.65	0.32	-0.13	0.74	1.00	-0.08	0.23	0.06	0.32	0.36	0.06
RPS	-0.03	0.10	0.98	0.16	-0.08	1.00	0.26	0.69	0.12	0.07	0.97
SB	0.05	0.13	0.26	0.48	0.23	0.26	1.00	0.23	0.19	-0.02	0.34
TB	0.15	0.20	0.73	0.34	0.06	0.69	0.23	1.00	0.08	0.33	0.78
VS	0.32	0.22	0.06	0.29	0.32	0.12	0.19	0.08	1.00	0.41	0.17
TS	0.50	0.36	0.03	0.32	0.36	0.07	-0.02	0.33	0.41	1.00	0.20
ALL	0.13	0.20	0.97	0.36	0.06	0.97	0.34	0.78	0.17	0.20	1.00

Table 4: Correlation in scale factor between all pairs of objects in Scenario *S*1 with size estimation via *m*1.

Scenarios	$m1$	$m2$	$m3$
$S1$	0.6567	0.7087	0.7220
$S2$	0.8174	0.7621	0.7936
$S3$	0.9651	0.9660	0.9698

Table 5: Index of fuzziness of $FOM(B)$ for the three scenarios and three measures of size via $m1$, $m2$, and $m3$.

The index of fuzziness values $h(FOM(B))$ are listed in Table 5 for scenarios $S1$-$S3$ and for measures $m1$-$m3$. These values provide a quantitative support for the qualitative observation derived from Figs. 2 and 3.

4. CONCLUSIONS

With a view to complement the existing rich statistical shape modeling literature, in this paper, we have introduced a fuzzy alternative to object modeling. Starting off from our preliminary work in [20, 21], our motivation behind fuzzy object modeling is to tightly integrate *FOMs* with the fuzzy connectedness machinery for building hybrid strategies and thereby to arrive at practical solutions to the *AAR* problem. In this paper, we have addressed some aspects of the fuzzy model building operation. The hierarchical organization H of the objects, the hierarchy in the building process, and the hierarchical information contained in ρ and λ are all important, in addition to the set $\mathcal{M}$ of fuzzy models, in our approach. We gave some supporting evidences for the ideas behind hierarchy from the viewpoint of model building. Our future work will include other body regions, means for bringing them into an integrated hierarchical mold, and object recognition and delineation strategies for *AAR*.

Other alignment strategies, including image/structure registration methods, may offer better *FOMs* than those proposed in this paper. From a theoretical perspective, there are two important considerations to address: (a) $7LN$ free parameters to deal within registration; (b) the fuzzy model FM_ℓ to satisfy the hierarchy in terms of offspring-to-parent (fuzzy) containment and the mutual exclusivity of models corresponding to siblings at each level of H.

5. ACKNOWLEDGEMENTS

This work is partially supported by a DHHS grant HL105212.

6. REFERENCES

[1] Torigian, D.A. and Alavi, A.: "The evolving role of structural and functional imaging in assessment of age-related changes in the body," *Seminars in Nuclear Medicine*, 37, 64-68 (2007).
[2] Kass, M., Witkin, A. and Terzopoulos, D.: "Snakes: Active contour models," *Communications of the ACM*, 14, 335-345 (1987).
[3] Xu, C. and Prince, J.: "Snakes, shapes, and gradient vector flow," *IEEE Transactions on Image Processing*, 7, 359-369 (1998).
[4] Falcao, A., Udupa, J.K., Samarasekera, S., Sharma, S., Hirsch, B., and Lotufo, R.: "User-steered image segmentation paradigms: Live wire and live lane," *Graphical Models and Image Processing*, 60, 233-260 (1998).
[5] Malladi, R., Sethian, J., and Vemuri, B.: "Shape modeling with front propagation: A level set approach," *IEEE Transactions on Pattern Analysis and Machine Intelligence*, 17, 158-175 (1995).
[6] Boykov, Y., Veksler, O., and Zabih, R.: "Fast approximate energy minimization via graph cuts," *IEEE Transactions on Pattern Analysis and Machine Intelligence*, 23, 1222-1239 (2001).
[7] Udupa, J.K. and Samarasekera, S.: "Fuzzy connectedness and object definition: Theory, algorithms and applications in image segmentation," *Graphical Models and Image Processing*, 58, 246-261 (1996).
[8] Beucher, S.: "The watershed transformation applied to image segmentation," *10th Pfefferkorn Conference on Signal and Image Processing in Microscopy and Microanalysis*, pp. 399-314 (1992).

[9] Mumford, D. and Shah, J.: "Optimal approximation by piecewise smooth functions and associated variational problems," *Communications of Pure and Applied Mathematics*, 42, 577-685 (1989).
[10] Cootes, T., Taylor, C., and Cooper, D.: "Active shape models – Their training and application," *Computer Vision and Image Understanding*, 61, 38-59 (1995).
[11] Pizer, S.M., Gerig, G., Joshi, S.C., and Aylward, S.R.: "Multiscale medial shape-based analysis of image objects," *Proceedings of the IEEE*, 91(10), 1670-1679 (2003).
[12] Thompson, P. and Toga, A.: "Detection, visualization and animation of abnormal anatomic structures with a probabilistic brain atlas based on random vector field transformations," *Medical Image Analysis*, 1, 271-294 (1997).
[13] Wang, W., D'Agostino, E., Seghers, D., Maes, F., Vandermeulen, D., and Suetens, P.: "Large-scale validation of non-rigid registration algorithms for atlas-based brain image segmentation," *Proceedings of SPIE*, 6144, 61440S-61447S (2006).
[14] Ashburner, J. and Friston, K.: "Unified Segmentation," *NeuroImaging*, 15(13), 839-851 (2005).
[15] Pohl, K.M., Fisher, J., Grimson, W.E.L., Kikinis, R., and Wells, W.M.: "A Bayesian model for joint segmentation and registration," *NeuroImage*, 31, 228-239 (2006).
[16] Rousson, M. and Paragios, N.: "Prior knowledge, level set representations and visual grouping," *International Journal of Computer Vision*, 76, 231-243 (2008).
[17] Liu, L. and Udupa, J.K..: "Oriented active shape models," *IEEE Transactions on Medical Imaging*, 28(4), 571-584 (2009).
[18] Tu, Z., Narrr, K.L., Dollar, P., Dinov, I., Thompson, P.M., and Toga, A.W.: "Brain anatomical structure segmentation by hybrid discriminative/generative models," *IEEE Transactions on Medical Imaging*, 27(4), 495-509 (2008).
[19] Lotjonen, J.M.P., Wolz, R., Koikkalainen, J.R., Thurfjell, L., Waldemar, G., Soininen, H., and Rueckert, D.: "Fast and robust multi-atlas segmentation of brain magnetic resonance images," *Neuroimaging*, 49, 2352-2365 (2010).
[20] Miranda, P.A.V., Falcao, A.X., and Udupa, J.K.:"Clouds: A model for synergistic image segmentation," *Proceedings of the ISBI*, pp 209-212, Paris, France, May 14-17, (2008).
[21] Miranda, P.A.V., Falcao, A.X. and Udupa, J.K.: "Cloud Bank: A Multiple Clouds Model and Its Use in MR Brain Image Segmentation." *The Sixth IEEE International Symposium on Biomedical Imaging: from Nano to Macro* (ISBI), Boston MA, ISBN 978-1-4244-3932-4/09, doi: 10.1109/ISBI. 2009, 5193095, *IEEE*, June 28th – July 1st, pp. 506-509, (2009).
[22] Kaufman, A.: *Introduction to the Theory of Fuzzy Subsets*, volume 1, Academic Press: New York, NY (1975).
[23] Raya, S.P., and Udupa, J.K.: "Shape-based interpolation of multidimensional objects" *IEEE Transactions on Medical Imaging*, MI-9(1), 32-42 (1990).
[24] Ciesielski, K.C., Chen, X, Udupa, J.K., and Grevera, G.J.: "Linear time algorithms for exact distance transform," *Journal of Mathematical Imaging and Vision*, 39, 193-209 (2011).
[25] Ciesielski, K.C., Udupa, J.K., Saha, P.K., and Zhuge, Y: "Iterative relative fuzzy connectedness for multiple objects with multiple seeds," *Computer Vision and Image Understanding*, 107(3), 160-182 (2007).